

Round-core-radius Dependent Electromagnetic Coupling of Multi-filament Helical Superconducting Tapes in a Swept Magnetic Field

Yoichi Higashi and Yasunori Mawatari

Abstract—With the excitation and demagnetization of a magnet for magnetic resonance imaging in mind, we theoretically and numerically investigated electromagnetic coupling—especially its dependence on the round-core radius R —of multi-filament helically wound superconducting tapes under steady-state conditions in a constantly ramped magnetic field. We found that even in a rapidly ramped magnetic field, the electromagnetic coupling can be suppressed by reducing R to close to the tape width. We also clarified that the coupling sweep rate at which the electromagnetic coupling starts scales as R^{-2} , showing that the dependence on R reflects the penetration of magnetic flux from the edges of the tape. Even when the round core is as narrow as the tape width, the behavior is considered to be similar to the electromagnetic response of a flat tape rather than that of a tubular wire.

Index Terms—Electromagnetic coupling, multi-filament helical superconducting tape, magnetization loss, ramped magnetic field, numerical modeling.

I. INTRODUCTION

CORC (Conductor on Round Core) wire, which comprises a rare-earth barium copper oxide $\text{YBa}_2\text{Cu}_3\text{O}_{7-\delta}$ coated conductor on a round core [1], [2], is a promising candidate for superconducting (SC) wires for applications involving high-field magnets. Among all high-temperature SC cables and wires, CORC ones have the shortest pitch lengths, as short as several tens of millimeters. As such, the electromagnetic (EM) coupling between SC filaments through a plated thermally stabilizing layer is expected to be suppressed, and striation can facilitate further loss reduction. Some previous studies fabricated CORC cables made of striated coated conductors and evaluated their alternating-current losses experimentally [3], [4], but the SC filaments were completely separated by striation; that is, they were insulated. Regarding local heating in the SC filaments, a copper stabilizing layer is coated on top of the multi-filament tapes for increased thermal stability. Very recently, a spirally twisted multi-filament coated conductor with finite transverse conductance between the SC filaments was fabricated, and measurements were made regarding how the magnetization losses depended on the frequency of a sinusoidally oscillating applied field [5]. At low transverse field amplitudes, selective measurements were made of the dominant contribution from coupling losses to the magnetization loss to determine the coupling time constants [5].

Y. Higashi and Y. Mawatari are with National Institute of Advanced Industrial Science and Technology (AIST), Tsukuba, Ibaraki 305-8568, Japan (e-mail: y.higashi@aist.go.jp).

Manuscript received mmmm dd, yyyy; revised mmmm dd, yyyy.

Regarding theoretical studies, based on the thin-sheet approximation using the current vector potential, EM analyses have been performed to investigate the magnetization loss and EM coupling in a sinusoidally oscillating applied field [6]–[8]. Numerical simulation has shown considerable reduction of the magnetization loss by striation in high magnetic fields, although an increase was seen in the magnetization loss in low fields when there were only a few filaments [6].

Despite the aforementioned studies, how the EM coupling depends on the core radius remains unclear and is yet to be investigated systematically. Clarifying the conditions for the EM coupling would give valuable information about how fast an applied field can be swept given the practical parameters of the CORC cable or wire. As opposed to previous theoretical studies [6]–[8], we consider a swept magnetic field with the excitation and demagnetization of a magnetic resonance imaging (MRI) magnet in mind.

In the present study, we use numerical simulations to investigate the magnetization loss and EM coupling of a multi-filament helical SC tape in an applied magnetic field with a high sweep rate of $\beta = 300$ mT/s, which is two orders of magnitude higher than a typical sweep rate of an MRI magnet; in particular, we focus on the dependence on the core radius. We assume, for example, the fast demagnetization of an MRI magnet during an emergency stop.

II. MODEL OF MULTI-FILAMENT HELICAL SUPERCONDUCTING TAPE

We examine numerically the model of a four-filament helical SC tape with conductors of finite normal resistivity ρ_n embedded in slots between the filaments. We assume that the coupling current between the SC filaments flows uniformly through the thermal stabilizing layer. The stabilizer information (e.g., conductivity, thickness, and effective length responsible for the transverse conductance) can be incorporated via the transverse conductivity (resistivity) $\sigma_n = 1/\rho_n$ as discussed in Section III, thereby reducing a three-dimensional model to a two-dimensional model [9]. Here, we model a thermal stabilizer such as copper on top of the SC filaments by means of a finite-resistivity conductor as in Refs. [9]–[11]. Fig. 1 shows the four-filament helical SC tape schematically. Unless specified otherwise, the dimensions are as follows: the total tape width is $w_0 = 2$ mm, the width of an SC filament is $w_1 = 0.485$ mm, the slot width is $s_1 = 20$ μm , the thickness of the SC tape is $d_0 = 2$ μm , and the radius of the hollow cylinder is $R = 3$ mm.

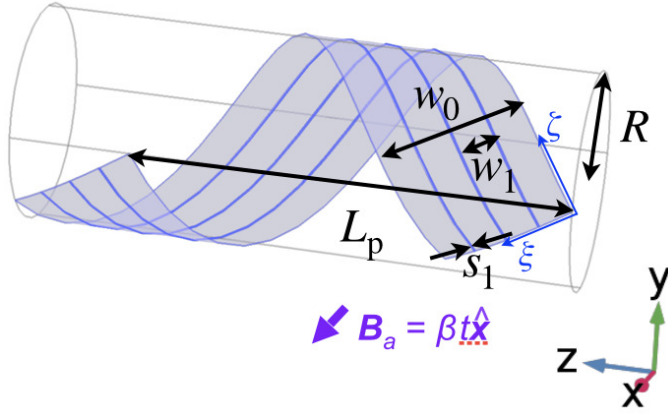


Fig. 1. Schematic of four-filament helically wound superconducting (SC) tape of total width w_0 , filament width w_1 , resistive slot width s_1 , and pitch L_p on a hollow cylinder of radius R . The axes (ξ, ζ) are on the tape surface.

The helical SC tape is assumed to be so thin ($d_0 \ll w_0$) that it can be approximated as an infinitesimally thick surface described by the coordinates [12]

$$\begin{cases} x = R \cos[(k\zeta - \xi/R)/\sqrt{1 + (kR)^2}], \\ y = R \sin[(k\zeta - \xi/R)/\sqrt{1 + (kR)^2}], \\ z = (\zeta + kR\xi)/\sqrt{1 + (kR)^2}, \end{cases} \quad (1)$$

where $k = 2\pi/L_p$ and L_p is the pitch length of the helical conductor. The axial coordinates (ξ, ζ) are orthogonal on the tape surface. We consider the helical SC tape surface with a full conductor pitch L_p spanned by $-w_0/2 \leq \xi \leq w_0/2$ and $-L_{\text{tape}}/2 \leq \zeta \leq L_{\text{tape}}/2$, with $L_{\text{tape}} = L_p\sqrt{1 + (kR)^2}$ being the tape length (see Figs. 1 and 2).

III. RESPONSE OF MULTI-FILAMENT HELICAL TAPE TO A RAMPED FIELD

Because an MRI magnet operates in a magnetic field as high as a few teslas, we may assume that the parts of the SC tape that are perpendicular to the applied field are fully penetrated by magnetic flux vortices. For a concrete estimate, in a multi-filament helical tape, the full penetration field can be estimated using the formula for a flat tape, namely, $B_p = (\mu_0 J_c d_0 / \pi) [1 + \ln(w_1/d_0)] \approx 0.260 \text{ T}$ [13], where μ_0 is the magnetic permeability of a vacuum and J_c is the critical current density. Meanwhile, in the parts of the tape that are parallel to the applied field, the perpendicular field component is small and does not reach B_p , and the loss generated in such parts is negligibly small.

In the fully penetrated state, the spatial profile of the magnetic field on the SC tape does not change, being kept in the steady state, as long as we disregard the magnetic field and its angle dependence of J_c ; that is, J_c is constant. The approximation of constant J_c is effective for evaluating the power loss [14].

At high fields, magnetization losses dominate transport losses [15], and so we neglect the contribution from transport losses in the present study. We also neglect the magnetic field due to the screening current because it is much smaller than the applied field.

In previous work, by adopting the thin-sheet approximation that takes account of only the perpendicular field component, we derived the steady-state Faraday–Maxwell equation for a constantly swept applied magnetic field $\mathbf{B}_a = \beta t \hat{x}$ with rate $\beta = d\mathbf{B}_a/dt$ [12], [14]. We base the present numerical simulation on the following two-dimensional Faraday–Maxwell equation on the tape surface (ξ, ζ) extended to multi-filament helical SC tapes:

$$\frac{\partial}{\partial \xi} \left(\rho \frac{\partial g}{\partial \xi} \right) + \frac{\partial}{\partial \zeta} \left(\rho \frac{\partial g}{\partial \zeta} \right) = \beta \cos \left[\frac{k\zeta - \xi/R}{\sqrt{1 + k^2 R^2}} \right], \quad (2)$$

where $g(\xi, \zeta)$ a scalar function defined on the helical SC tape surface. The contour lines of $g(\xi, \zeta)$ describe the current streamlines on the helical tape surface (see Fig. 2).

To model a multi-filament helical SC tape, we adopt the SC nonlinear resistivity ρ_{sc} and the transverse linear one ρ_n for the filaments and slots, respectively, namely,

$$\rho(\xi, \zeta) = \begin{cases} \frac{E_c}{J_c} \left(\frac{|\mathbf{J}(\xi, \zeta)|}{J_c} \right)^{n-1} \equiv \rho_{\text{sc}}(|\mathbf{J}|) & \text{for SC filaments,} \\ \rho_n & \text{for resistive slots,} \end{cases} \quad (3)$$

which is defined via the electric field \mathbf{E} –current density \mathbf{J} characteristic of $\mathbf{E} = \rho \mathbf{J}$. Herein, we disregard the dependence of J_c on the the magnetic field and its angle. We set $J_c = 5 \times 10^{10} \text{ A/m}^2$, $E_c = 1 \text{ } \mu\text{V/cm}$ for the electric field, and $n = 15$ in the power of the SC nonlinear resistivity. We incorporate the effect of a copper thermal stabilizer on the multi-filament helical SC tape through ρ_n [9], [11]. The transverse conductance is obtained as $G_n = \sigma_n (L_{\text{tape}}/2) d_0 / s_1$, where we use the effective tape length $L_{\text{tape}}/2$ (see Fig. 2). Consequently, the transverse conductance per unit length is $G_t = G_n / (L_{\text{tape}}/2) = \sigma_n d_0 / s_1$. When the coupling current flows mainly through the copper stabilizer plated on the multi-filament helical tape, we can equate G_t with the conductance per unit length via the plated copper stabilizer, namely, $G_{\text{Cu}} = \sigma_{\text{Cu}} d_{\text{Cu}} / l_{\text{Cu}}$, where σ_{Cu} is the conductivity of copper, d_{Cu} is the thickness of the plated copper, and l_{Cu} is the effective length responsible for the transverse conductance via the plated copper layer. Therefore, by adopting $d_{\text{Cu}} = 20 \text{ } \mu\text{m}$, $l_{\text{Cu}} = 300 \text{ } \mu\text{m}$ [9], and $\sigma_{\text{Cu}} = 5 \times 10^8 \text{ } \Omega^{-1}\text{m}^{-1}$ at 77 K [16], we have that

$$\sigma_n = \frac{s_1 d_{\text{Cu}}}{d_0 l_{\text{Cu}}} \sigma_{\text{Cu}} \approx 3.33 \times 10^8 \text{ } \Omega^{-1}\text{m}^{-1}, \quad (4)$$

which yields $\rho_n \sim 1 \times 10^{-9} \text{ } \Omega\text{m}$, and we use this value throughout the paper.

IV. NUMERICAL RESULTS

A. Current Streamlines

To obtain the solution for $g(\xi, \zeta)$, we solve Eq. (2) numerically using the commercial software COMSOL Multiphysics® [17]. We impose the Dirichlet boundary condition $g(\xi = \pm w_0/2, \zeta) = 0$ along the long edges of the tape, and we impose the periodic boundary condition

$$g(\xi, \zeta = -L_{\text{tape}}/2) = g(\xi, \zeta = L_{\text{tape}}/2) \quad (5)$$

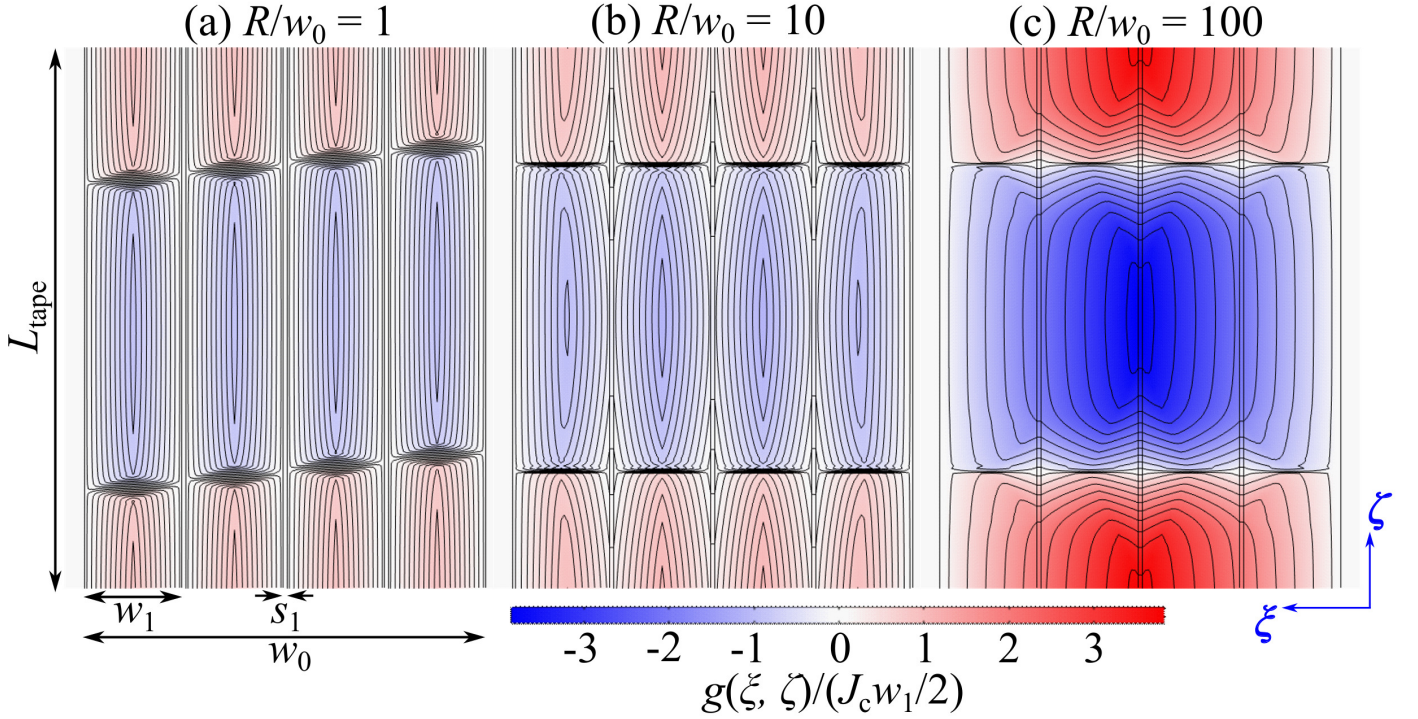


Fig. 2. Current streamlines and spatial profile of $g(\xi, \zeta)$ on surface of multi-filament helical SC tape for $R/w_0 =$ (a) 1, (b) 10, and (c) 100. The pitch length and sweep rate are $L_p = 6$ mm and $\beta = 300$ mT/s, respectively, and the tape length for a full pitch is $L_{\text{tape}} \approx$ (a) 13.9, (b) 125.8, and (c) 1256.7 mm.

on the terminals of the whole tape. The ξ and ζ components of the current density on the tape surface are obtained from the spatial derivatives of $g(\xi, \zeta)$ as [12]

$$J_\xi = -\frac{\partial g(\xi, \zeta)}{\partial \zeta}, \quad J_\zeta = \frac{\partial g(\xi, \zeta)}{\partial \xi}. \quad (6)$$

In Fig. 2, the solid lines depict the current streamlines on the tape surface, and the color scale shows the profile of the scalar function $g(\xi, \zeta)/(J_c w_1/2)$. At $R/w_0 = 1$ [Fig. 2(a)], each SC filament is completely decoupled electrically. However, partial EM coupling appears at $R/w_0 = 10$ [Fig. 2(b)] because the current streamlines go partially across the resistive slots. At $R/w_0 = 100$ [Fig. 2(c)], the current streamlines spread throughout the tape surface, and thus the SC filaments are completely coupled electrically. As shown in Fig. 2, the helical winding divides the current streamlines into closed loops for every half pitch, showing that the effective tape length is $L_{\text{tape}}/2$. However, unlike for multi-filament twisted tapes [11], note that for the parameters adopted in the present study, one cannot obtain the correct solution for $g(\xi, \zeta)$ at least when $R/w_0 = 1$ if the Dirichlet boundary condition $g(\xi, \zeta = \pm L_{\text{tape}}/4) = 0$ is imposed where the tape is parallel to the applied field ($\parallel \hat{x}$).

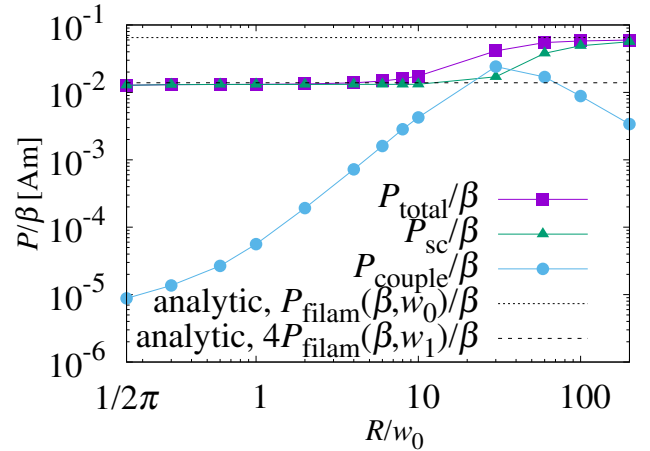


Fig. 3. Dependence of loss power per unit tape length on hollow-cylinder radius for $L_p = 6$ mm. P_{total} , P_{sc} , and P_{couple} represent the total, SC, and coupling loss power, respectively. The field sweep rate is fixed to $\beta = 300$ mT/s. The dotted and dashed lines show the loss power evaluated analytically by $P_{\text{filam}}(\beta, w_0)/\beta$ and $4P_{\text{filam}}(\beta, w_1)/\beta$ [Eq. (11)], respectively.

B. Power Dissipation: Dependence on Cylinder Radius

The power dissipated on the tape surface per unit length is given by [11], [12]

$$P_{\text{total}} = P_{\text{sc}} + P_{\text{couple}}, \quad (7)$$

$$P_{\text{sc}} = \int \int_{\text{filaments}} d\xi d\zeta p(\xi, \zeta), \quad (8)$$

$$P_{\text{couple}} = \int \int_{\text{slots}} d\xi d\zeta p(\xi, \zeta), \quad (9)$$

$$p(\xi, \zeta) = \frac{d_0}{L_{\text{tape}}} \rho(\xi, \zeta) \left[\left(\frac{\partial g}{\partial \xi} \right)^2 + \left(\frac{\partial g}{\partial \zeta} \right)^2 \right]. \quad (10)$$

Fig. 3 shows the cylinder-radius dependence of the loss power relative to β for $L_p = 6$ mm and $\beta = 300$ mT/s. The total loss begins to increase at $R/w_0 \sim 10$. Even when the pitch length is a few times the tape width, for $R \gtrsim 10w_0$ in a rapidly ramped magnetic field with $\beta = 300$ mT/s, the SC filaments are coupled electrically with each other and the striation is ineffective. However, in a rapidly ramped field, we can suppress the EM coupling by winding the SC tape with a thin round core up to $R/w_0 \sim 1$. Therefore, in the CORC wire region (i.e., $R/w_0 \sim 1$), striation is effective for reducing the total loss.

For an effective tape width w , by taking the thin-filament limit of $w/R \rightarrow 0$, we obtain the following analytical formula for the loss power per unit length [12], which coincides with that for a twisted tape [14]:

$$P_{\text{filam}}(\beta, w) = \frac{B(\frac{2n+1}{2n}, \frac{1}{2})}{\pi} \left(\frac{\beta w}{2E_c} \right)^{\frac{1}{n}} \frac{J_c d_0 w^2 \beta}{2(2+1/n)}, \quad (11)$$

where $B(p, q) = 2 \int_0^{\pi/2} d\theta \cos^{2p-1} \theta \sin^{2q-1} \theta$ is the beta function with positive real numbers p and q .

For $R/w_0 \gtrsim 100$, the long L_{tape} means that the SC resistance $R_{\text{sc}}^{\parallel}$ becomes large relative to the transverse resistance R_n because $R_{\text{sc}}^{\parallel} \propto L_{\text{tape}}$, but $R_n \propto L_{\text{tape}}^{-1}$. Therefore, the coupling current flows from the SC filaments to the resistive slots, resulting in the EM coupling of the SC filaments. In this case, we have $w \approx w_0$, and the analytical values of $P_{\text{filam}}(\beta, w_0)/\beta$ agree well with the numerical ones (dotted line in Fig. 3). Here, we note that increasing the ratio of the round core radius to the total tape width, R/w_0 , does not necessarily indicate the thick cable with $R \sim$ a few hundred millimeters. Reducing w_0 also gives rise to an increase of R/w_0 , although we fix w_0 and change R in the present study.

Meanwhile, for $R/w_0 \lesssim 1$, $R_{\text{sc}}^{\parallel}$ remains small relative to R_n . Thus, no EM coupling occurs, and we have $w \approx w_1$. The analytical values given by $4P_{\text{filam}}(\beta, w_1)/\beta$ agree well with the numerical ones (dashed line in Fig. 3); here, the factor 4 comes from the number of SC filaments.

C. Power Dissipation: Dependence on Sweep Rate

Fig. 4 shows how the total loss power relative to β depends on the field sweep rate β for $L_p = 6$ mm when R is changed. For $\beta_{\text{MRI}} \sim 1$ mT/s, a typical sweep rate for an MRI magnet [18], [19], there is no EM coupling for $R/w_0 \lesssim 10$. However, in a rapidly swept field with $\beta \sim 100$ mT/s, the striation is effective for reducing the loss only when $R/w_0 \sim 1$. For $R/w_0 \gtrsim 10$, the total loss increases slightly, meaning that the striation is ineffective even in the case of a short pitch of $L_p/w_0 = 3$.

For large β , w_0 is viewed as being the effective tape width because of the EM coupling. Thus, in the case of $R/w_0 = 100$, the loss power at $\beta = 1000$ mT/s shows quantitatively good agreement with $P_{\text{filam}}(\beta, w_0)/\beta$ (dotted line in Fig. 4). Meanwhile, for small β , the effective tape width should be w_1 , and therefore $4P_{\text{filam}}(\beta, w_1)/\beta$ agrees well with the numerics (dashed line in Fig. 4) [20].

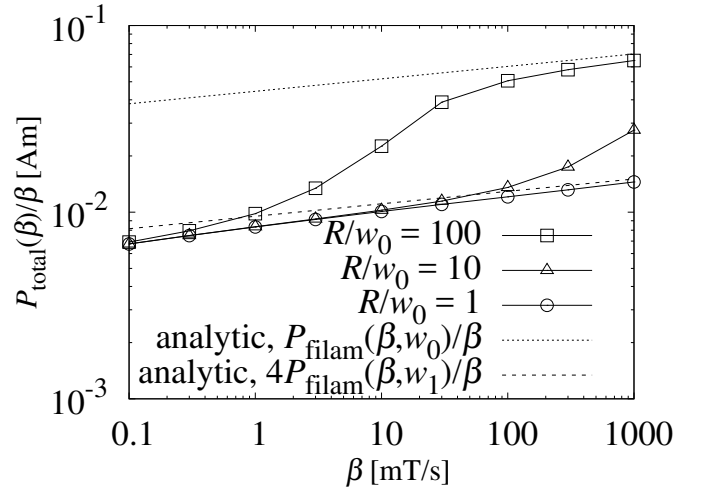


Fig. 4. Dependence of total loss power relative to β on field sweep rate β for $L_p = 6$ mm. The dotted and dashed lines show the loss power evaluated analytically by $P_{\text{filam}}(\beta, w_0)/\beta$ and $4P_{\text{filam}}(\beta, w_1)/\beta$ [Eq. (11)], respectively.

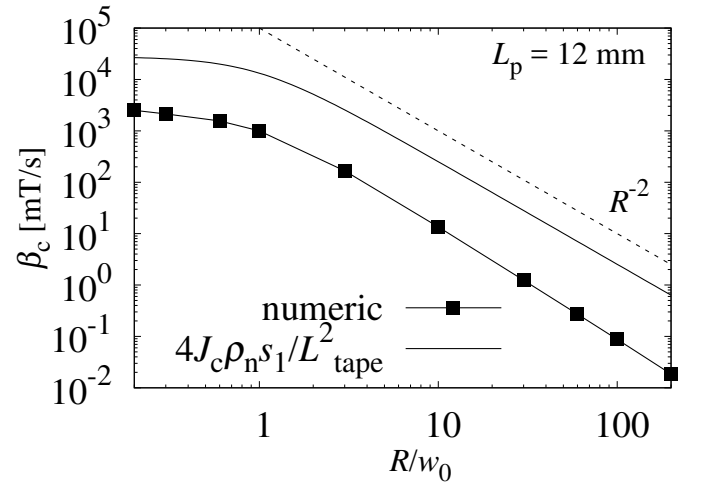


Fig. 5. Dependence of coupling sweep rate β_c on round-core radius R for $L_p = 12$ mm. The squares denote the numerical results, while the solid line with no symbols denotes the analytical result of Eq. (13).

V. DISCUSSION

A. Electromagnetic coupling

We examine the mechanism for EM coupling in a multi-filament helical tape in the similar way as in Ref. [11] by evaluating the coupling sweep rate β_c , where the EM coupling starts. Fig. 5 shows how β_c depends on the hollow-cylinder radius for $L_p = 12$ mm. Here, β_c is defined as β satisfying $P_{\text{couple}}(\beta)/P_{\text{sc}}(\beta) \approx 0.02$, and it is obtained numerically by subjecting β to linear interpolation (the squares in Fig. 5). The choice of $P_{\text{couple}}/P_{\text{sc}}$ affects the numerical results for β_c but is irrelevant for the R dependence, which is our interest here. We can understand how β_c depends on R by evaluating β_c analytically from the EM coupling condition, namely,

$$\frac{R_{\text{sc}}^{\parallel}}{R_n} = \frac{\beta}{\beta_c} > 1. \quad (12)$$

Herein, the SC filament resistance in the longitudinal (ζ) direction can be evaluated as $R_{sc}^{\parallel} = \rho_{sc}(L_{\text{tape}}/2)/w_1 d_0$.

For a nearly flat tape with a thick round core with $R/w_0 \gg 1$, the length scale at which magnetic flux vortices enter a superconductor can be viewed as being the filament width w_1 , and therefore the electric field in the superconductor is evaluated as $\sim \beta w_1$ (e.g., Ref. [21] for the disk geometry). Consequently, the SC resistivity is evaluated as $\rho_{sc} \sim \beta w_1 / J_c$. The transverse normal resistance is $R_n = \rho_n s_1 / (L_{\text{tape}}/2) d_0$. Therefore, we obtain the coupling sweep rate in the case of $R/w_0 \gg 1$ as

$$\beta_c \sim \frac{4J_c \rho_n s_1}{L_{\text{tape}}^2} \rightarrow \frac{J_c \rho_n s_1}{\pi^2 R^2} \propto R^{-2} \quad (kR \gg 1). \quad (13)$$

Meanwhile, in the case of a nearly tubular wire with a thin round core ($R/w_0 \sim 1$), the characteristic length scale of the flux motion can be viewed as being the core radius R , and therefore the electric field is evaluated as $\sim \beta R$, leading to $\rho_{sc} \sim \beta R / J_c$. Therefore, the coupling sweep rate in the case of $R/w_0 \sim 1$ is estimated as

$$\beta_c \sim \frac{4J_c \rho_n s_1}{L_{\text{tape}}^2} \frac{w_1}{R} \rightarrow \frac{J_c \rho_n s_1 w_1}{\pi^2 R^3} \propto R^{-3} \quad (kR \gg 1). \quad (14)$$

In Fig. 5, the solid line with no symbols corresponds to β_c evaluated analytically by Eq. (13). Here, β_c scales as R^{-2} for $R/w_0 \gg 1$, and its dependence on R agrees well with the numerics in the whole range of R . In the case of the nearly tubular wire with $R/w_0 \sim 1$, as estimated by Eq. (14) for $R/w_0 \gg 1$, β_c scales as R^{-3} , in disagreement with the numerics. Based on how β_c depends on R , we conclude that the EM coupling of a multi-filament helical tape reflects the penetration of magnetic flux from the long edges of the SC filaments.

B. Relation to coupling time constant

The measurement of ac losses for a fixed low amplitude of a sinusoidally oscillating applied magnetic field with sweeping a frequency f as in Refs. [5], [7] could be comparable to our calculations in which an applied field is actually swept at a constant rate β . Note that ac loss measurements for a fixed f with sweeping an applied field as in Ref. [6] is never comparable to our simulations. Alternating-current losses at low fields and high frequencies are dominated by coupling losses because the energy dissipation inside superconductors is negligible at sufficiently low fields. In the case of a sinusoidally oscillating magnetic field, the coupling time constant is given by $\tau_c = 1/2\pi f_c$ with the coupling frequency f_c . In this case, the coupling field sweep rate can be viewed as $2\pi f_c B$, which is corresponding to β_c in our notation; $\beta_c \equiv 2\pi f_c B$. Here, note that B denotes the magnetic field on the SC tape. Therefore, in the case of $R/w_0 \gg 1$ by using the estimation of β_c (13), we may relate the coupling time constant to the round core radius as

$$\tau_c \sim \frac{\mu_0 [L_p^2 + (2\pi R)^2]}{4\pi \rho_n} \left(\frac{d_0}{s_1} \right), \quad (15)$$

where μ_0 the vacuum permeability and the magnetic field on the SC tape is evaluated as $B \sim \mu_0 J_c d_0 / \pi$ based on the Bean

model. The estimation (15) can be obtained via the same way as in Ref. [11] in the case of an alternating-current field. One can immediately see from the relation (15) that with increasing R the time scale for a decaying coupling current becomes long, meaning that EM coupling starts from at low frequencies.

C. Effects of multi layers and tapes

We consider that SC tapes are subjected to an applied magnetic field as high as a few tesla, which is far above a full flux penetration field B_p . For concreteness, B_p for striated helical tapes is approximately estimated via the flat tape formula for the filament width w_1 ; $B_p = (\mu_0 J_c d_0 / \pi) [1 + \ln(w_1/d_0)] \approx 0.260$ T [13]. In the case of the multi-layer configuration, B_p will be a few times more than that for a single flat tape, but it is still much smaller than a few tesla. Accordingly, the magnetic flux penetrates the tapes completely. In this condition, because the response to an applied field is dominant, the interaction between SC tapes is relatively small and negligible. Therefore, the EM coupling among SC filaments in the tapes is not seriously influenced by the interaction between the striated SC tapes in the different layers. However, at low magnetic fields, the interaction between the tapes in the different layers might be important to model a CORC wire wound by several tapes and layers [6], [22].

VI. SUMMARY

Regarding the excitation and demagnetization of an MRI magnet, we simulated numerically the magnetization loss of a multi-filament helical SC tape in the steady state in a constantly ramped magnetic field. Even in a rapidly ramped field with a rate of $\beta = 300$ mT/s, no EM coupling of the SC filaments was seen for $R/w_0 \sim 1$ because of the short pitch length. However, for $R \gtrsim 10w_0$, the SC filaments were coupled electrically, showing the striation to be ineffective. The coupling sweep rate scaled as R^{-2} for $R/w_0 \gtrsim 1$, reflecting the penetration of magnetic flux from the tape edges. This behavior is considered to be similar to the EM response of a flat tape rather than that of a tubular wire, even when the round core is as narrow as the tape width, which is nearly a tubular wire.

ACKNOWLEDGMENTS

We thank M. Vojenčiak (Slovak Academy of Sciences) for discussions during the 31st International Symposium on Superconductivity (ISS2018). We also thank N. Amemiya (Kyoto University) and Y. Yoshida (AIST) for providing us with the pre-publication manuscript of Ref. [5]. The present work is based on results obtained from a project commissioned by the New Energy and Industrial Technology Development Organization (NEDO).

REFERENCES

- [1] D. C. van der Laan, "YBa₂Cu₃O_{7- δ} coated conductor cabling for low ac-loss and high-field magnet applications," *Supercond. Sci. Technol.*, vol. 22, no. 6, p. 065013, 2009.

- [2] J. D. Weiss, T. Mulder, H. J. ten Kate, and D. C. van der Laan, "Introduction of CORC[®] wires: highly flexible, round high-temperature superconducting wires for magnet and power transmission applications," *Supercond. Sci. Technol.*, vol. 30, no. 1, p. 014002, 2016.
- [3] J. Šouc, F. Gömöry, J. Kováč, R. Nast, A. Jung, M. Vojenčiak, F. Grilli, and W. Goldacker, "Low AC loss cable produced from transposed striated CC tapes," *Supercond. Sci. Technol.*, vol. 26, no. 7, p. 075020, 2013.
- [4] M. Vojenčiak, A. Kario, B. Ringsdorf, R. Nast, D. C. van der Laan, J. Scheiter, A. Jung, B. Runtsch, F. Gömöry, and W. Goldacker, "Magnetization ac loss reduction in HTS CORC[®] cables made of striated coated conductors," *Supercond. Sci. Technol.*, vol. 28, no. 10, p. 104006, 2015.
- [5] Y. Li, D. H. Kim, S. Inoue, Y. Yoshida, T. Machi, and N. Amemiya, "Coupling Time Constant Measurements of Spirally-Twisted Striated Coated Conductors With Finite Transverse Conductance Between Filaments," *IEEE Trans. Appl. Supercond.*, vol. 30, no. 4, pp. 1–5, 2020.
- [6] Y. Wang, M. Zhang, F. Grilli, Z. Zhu, and W. Yuan, "Study of the magnetization loss of CORC[®] cables using a 3D T-A formulation," *Supercond. Sci. Technol.*, vol. 32, no. 2, p. 025003, 2019.
- [7] Y. Sogabe, Y. Mizobata, and N. Amemiya, "Coupling time constants and ac loss characteristics of spiral copper-plated striated coated-conductor cables (SCSC cables)," *Supercond. Sci. Technol.*, vol. 33, no. 5, p. 055008, 2020.
- [8] Y. Yan, P. Song, W. Li, J. Sheng, and T. Qu, "Numerical Investigation of the Coupling Effect in CORC Cable With Striated Strands," *IEEE Trans. Appl. Supercond.*, vol. 30, no. 4, pp. 1–5, 2020.
- [9] N. Amemiya, N. Tominaga, R. Toyomoto, T. Nishimoto, Y. Sogabe, S. Yamano, and H. Sakamoto, "Coupling time constants of striated and copper-plated coated conductors and the potential of striation to reduce shielding-current-induced fields in pancake coils," *Supercond. Sci. Technol.*, vol. 31, no. 2, p. 025007, 2018.
- [10] N. Amemiya, S. Sato, and T. Ito, "Magnetic flux penetration into twisted multifilamentary coated superconductors subjected to ac transverse magnetic fields," *J. Appl. Phys.*, vol. 100, no. 12, p. 123907, 2006.
- [11] Y. Higashi and Y. Mawatari, "Electromagnetic coupling of twisted multifilament superconducting tapes in a ramped magnetic field," *Supercond. Sci. Technol.*, vol. 32, no. 5, p. 055010, 2019.
- [12] Y. Higashi and Y. Mawatari, "Efficient Numerical Modeling of the Magnetization Loss on a Helically Wound Superconducting Tape in a Ramped Magnetic Field," *IEEE Trans. Appl. Supercond.*, vol. 30, no. 3, pp. 1–7, 2020.
- [13] E. H. Brandt, "Superconductors of finite thickness in a perpendicular magnetic field: Strips and slabs," *Phys. Rev. B*, vol. 54, pp. 4246–4264, 1996.
- [14] Y. Higashi, H. Zhang, and Y. Mawatari, "Analysis of Magnetization Loss on a Twisted Superconducting Strip in a Constantly Ramped Magnetic Field," *IEEE Trans. Appl. Supercond.*, vol. 29, no. 1, pp. 1–7, 2019.
- [15] K. Kajikawa, S. Awaji, and K. Watanabe, "Ac loss evaluation of an hts insert for high field magnet cooled by cryocoolers," *Cryogenics*, vol. 80, pp. 215 – 220, 2016, special Issue on HTS Cooling 2015.
- [16] H. Hucek, K. Wilkes, K. Hanby, and J. Thompson, "Handbook on materials for superconducting machinery," *Metals and Ceramic Information Center, Battelle, Columbus Laboratories, Columbus, OH*, 1977.
- [17] COMSOL Multiphysics[®]. [Online]. Available: www.comsol.com
- [18] S. Yokoyama, J. Lee, T. Imura, T. Matsuda, R. Eguchi, T. Inoue, T. Nagahiro, H. Tanabe, S. Sato, A. Daikoku, T. Nakamura, Y. Shirai, D. Miyagi, and M. Tsuda, "Research and Development of the High Stable Magnetic Field ReBCO Coil System Fundamental Technology for MRI," *IEEE Trans. Appl. Supercond.*, vol. 27, no. 4, pp. 1–4, 2017.
- [19] T. Yachida, M. Yoshikawa, Y. Shirai, T. Matsuda, and S. Yokoyama, "Magnetic Field Stability Control of HTS-MRI Magnet by Use of Highly Stabilized Power Supply," *IEEE Trans. Appl. Supercond.*, vol. 27, no. 4, pp. 1–5, 2017.
- [20] The simulated losses are smaller than the analytically evaluated values. This is because we put the numerical value in the current density to avoid numerical instabilities in the following way; $|\mathbf{J}(\xi, \zeta)|^2 = (J_\xi^2 + J_\zeta^2)/J_c^2 + \delta$ with $\delta = 10^{-1}$. However, the choice of $\delta = 10^{-1}$ results in somewhat smaller numerical value than analytically expected one; that is, magnetization losses are numerically underestimated. Especially, effect of δ becomes prominent when the current is small at low sweep rates β , and thereby this underestimation is pronounced. On the other hand, at high β , because the current is large, the δ in the current has relatively low impact. Thus the discrepancy between the numerical value and the analytical one becomes small as seen in Fig. 4 (Compare the discrepancy at high β with that at low β). Indeed, we confirmed the discrepancy tends to be somewhat small for $\delta = 0.6 \times 10^{-1}$, but the dependence of the loss power on β does not change qualitatively and our conclusion is not altered.
- [21] Y. Mawatari, A. Sawa, H. Obara, M. Umeda, and H. Yamasaki, "Field-sweep rate dependence of magnetization and current–voltage characteristics in superconducting disks," *Appl. Phys. Lett.*, vol. 70, no. 17, pp. 2300–2302, 1997.
- [22] M. Majoros, M. D. Sumption, E. W. Collings, and D. C. van der Laan, "Magnetization losses in superconducting YBCO conductor-on-round-core (CORC) cables," *Supercond. Sci. Technol.*, vol. 27, no. 12, p. 125008, 2014.